Application of integral equation theories to predict the structure of diatomic fluids

ARTICLE *in* THE JOURNAL OF CHEMICAL PHYSICS · MARCH 1995

Impact Factor: 2.95 · DOI: 10.1063/1.469468

2 AUTHORS, INCLUDING:

Leo Lue
University of Strathclyde
104 PUBLICATIONS **1,375** CITATIONS

Application of integral equation theories to predict the structure of diatomic fluids

Leo Lue and Daniel Blankschtein[a)]
Department of Chemical Engineering and Center for Materials Science and Engineering, Massachusetts Institute of Technology, Cambridge, Massachusetts 02139

(Received 14 November 1994; accepted 2 December 1994)

We compare the capabilities of the site–site Ornstein–Zernike equation and the Chandler–Silbey–Ladanyi equations to predict the fluid structure for: (i) fluids composed of homonuclear diatomic Lennard-Jones molecules, and (ii) fluids composed of nonpolar or polar heteronuclear diatomic Lennard-Jones molecules. In (i), we solve the site–site Ornstein–Zernike (SSOZ) equation with the Percus–Yevick (PY) closure, and the Chandler–Silbey–Ladanyi (CSL) equations with the hypernetted-chain (HNC) closure to predict the various pair correlation functions at various bond lengths, fluid densities, and temperatures. In general, we find that the CSL equations become more accurate, when compared with computer simulation results, as the bond length increases or as the density decreases, with temperature having no significant effect. In fact, at densities below the critical density, the fluid structure predictions of the CSL equations are found to be in closer agreement with the computer simulation results than those of the SSOZ equation. We also present a general method for computing the low-order density bridge functions in the context of the CSL equations. In the case of homonuclear diatomic molecules, the zeroth-order bridge functions, $B^{(0)}$, are found to have little effect on the pair correlation function predictions of the CSL equations. However, the addition of the first-order bridge functions, $B^{(1)}$, results in a significant improvement of these predictions. In general, the accuracy of the CSL equations, including the various bridge function corrections, is found to increase as the bond length increases or as the density decreases, similar to what we found when the HNC closure (in which the bridge functions are set equal to zero) was used. Finally, in (ii), we find that for nonpolar heteronuclear diatomic fluids, the CSL equations, with the HNC, HNC$+B^{(0)}$, and HNC$+B^{(1)}$ closures, perform very well in predicting the correlation functions between the larger interactions sites. For polar heteronuclear diatomic fluids, we find that the CSL equations seem to offer an improvement over the SSOZ equation. Once again, the CSL equations provide better predictions for the correlation function between the larger interaction sites.

I. INTRODUCTION

Interaction site models[1] have been used extensively to describe interactions between the molecules comprising a fluid. In these models, sites are located at various positions in a molecule, typically on atoms or groups of atoms. The interaction potential between two molecules is taken to be the sum of the interaction potentials between the various sites in each molecule. Specifically,

$$u(1,2)=\sum_{\alpha\gamma} u_{\alpha\gamma}(|r_\alpha - r_\gamma|), \tag{1}$$

where $u(1,2)$ is the interaction potential between molecules 1 and 2, $u_{\alpha\gamma}(r)$ is the interaction potential between site α located on molecule 1 and site γ located on molecule 2, and r_α (r_γ) is the position of site α (γ).

Given the intermolecular interaction potentials between the various species which exist in solution, one can determine solution thermodynamic properties through either Monte Carlo or molecular dynamics simulations of the system.[2] Although computer simulations constitute a powerful tool to analyze molecular systems, they display several shortcomings. Specifically, (i) the typical simulation time is very short (about 10^{-10} s), and (ii) there is a practical limit on the number of interaction sites that can be incorporated in the simulated system (about 10^4). Consequently, computer simulations are still unable to examine systems having long equilibration times or large length scales, such as self-assembling micellar solutions. In addition, these techniques are computationally intensive.

Integral equation theories, although less accurate than computer simulations, provide a powerful theoretical tool to analyze molecular systems. Indeed, they can offer a compromise between accuracy and computational expense, as well as avoid some of the computational difficulties encountered by computer simulations. Therefore, it appears both useful and important to examine in detail the extent of applicability of integral equation theories in the case of molecular fluids.

One particular integral equation, known as the site–site Ornstein–Zernike (SSOZ) equation, has found extensive use in the prediction of the structure and thermodynamic properties of interaction site fluids. This equation needs to be

[a)]Author to whom all correspondence should be addressed.

supplemented by a closure relation in order to be utilized. Typically, approximate closures borrowed from simple fluid theories have been utilized. However, this combination of the SSOZ equation with a simple fluid closure has led to several problems. For example, (i) the predicted dielectric constant is equal to that of an ideal gas, regardless of the nature of the fluid,[3,4] and (ii) the addition of auxiliary sites, that is, sites which do not interact with any other sites in the system, has been found[5,6] to alter the correlations between interactions sites, which is not physically reasonable. Moreover, probably the most serious problem associated with the SSOZ equation is that when it fails to yield physically reasonable predictions, there are no straightforward, systematic methods to improve its predictive accuracy.

A particularly useful avenue to remedy this situation has been to construct integral equations for interaction site fluids which are based on a diagrammatic expansion of the site–site total correlation function. Indeed, when the techniques of graph theory are applied to this problem, this results in a set of integral equations, known as the Chandler–Silbey–Ladanyi (CSL) equations.[7] These integral equations are[7] diagrammatically proper, in that, unlike the SSOZ equation,[8] they do not include diagrams which are not present in the exact theory. This new approach, however, entails difficulties of its own. The major one is that, similar to what is encountered in the theory of simple fluids,[9] a subset of these diagrams, known as the bridge diagrams, needs to be approximated. It is noteworthy, that the bridge diagrams make a greater contribution in the case of molecular fluids than they do in the case of simple fluids. Specifically, as the number of interaction sites in a given molecule increases, the number of missing diagrams increases.

The CSL equations with an approximate closure [hypernetted chain (HNC) and Percus–Yevick (PY)] were first applied[10] to systems composed of homonuclear diatomic Lennard-Jones molecules. Unfortunately, it was found that the predictions of the CSL-HNC and CSL-PY equations for the site–site pair correlation functions are less accurate than those of the SSOZ equation with similar closures. These initial findings, coupled with the mathematical complexities associated with solving the CSL equations, appear to have discouraged the further use of these equations in other situations.

Several years later, Lupkowski and Monson developed[11] a cluster perturbation based on the CSL equations. This formalism was applied to fluids composed of homonuclear diatomic molecules, as well as to dipolar hard-dumbbell molecules, to predict the fluid structure, thermodynamic properties, and phase behavior.[12–15] These new perturbation theories were found to perform well for these fluids. Nevertheless, there are two major problems associated with perturbation theories for molecular fluids. The first one involves the availability of accurate information about the structure and thermodynamics of the reference system in order for the results to be meaningful. Reference system properties are not known for interaction site fluids to the same extent to which they are known in the case of simple fluids. The second problem reflects the fact that the properties of the reference system may not necessarily be close to those of the system of interest. An important example is that of water, for which a natural reference system would consist of uncharged water molecules. However, such a reference system would have a very different structure from that of actual water. Both of these difficulties suggest that it would be useful to improve the CSL equations in a nonperturbative manner. Specifically, this involves finding better closure relations for the CSL equations.

The success of the CSL cluster-perturbation work led to a renewed interest in the CSL equations. We recently developed[16] explicit expressions for the residual Helmholtz free energy and the residual chemical potential in terms of the correlation functions, in the context of the CSL equations with a general closure. We also found[16] that the residual Helmholtz free energy satisfies a variational principle for a certain class of closure relations. Yethiraj applied[17] the CSL equations with the PY closure to tangent hard-sphere diatomic fluids, and found that they yield more accurate predictions of the fluid structure and thermodynamic properties than the SSOZ equation. Yethiraj and co-workers also applied[18] these equations to linear triatomic molecules, and once again found that the predictions of the CSL equations are superior to those of the SSOZ equation. These recent developments,[17,18] however, do not yet fully agree with computer simulation results, thus highlighting the need to find better closure relations for the CSL equations.

In this paper, we analyze and compare the predictions of the site–site pair correlation functions of both the SSOZ and CSL equations for various diatomic fluids in order to assess their respective ranges of validity and applicability. In addition, we present a new method to compute better approximations for the bridge functions, as well as examine the influence of these functions on the predictions of the CSL equations for the site–site pair correlation functions.

The remainder of the paper is organized as follows. In Sec. II, we briefly describe the SSOZ and CSL equations. In Sec. III, we present a discussion of the bridge functions, as well as of a method for computing approximations to the bridge functions. In Sec. IV, we compare the SSOZ and CSL predictions of the pair correlation functions corresponding to various homonuclear diatomic Lennard-Jones fluids with those of computer simulations in order to assess the relative accuracy of these equations. In addition, in Sec. IV, we apply the CSL and SSOZ equations to polar and nonpolar heteronuclear diatomic Lennard-Jones molecules and compare their predictive capabilities. Finally, in Sec. V, we present a summary and discussion of the main findings of the paper.

II. INTEGRAL EQUATIONS

A. The site–site Ornstein–Zernike equation

One of the first equations developed for interaction site fluids was the site–site Ornstein–Zernike (SSOZ) equation.[19] When written in momentum (k) space, it is given by[19]

$$\hat{h}(k)=\hat{w}(k)\hat{c}(k)\hat{w}(k)+\hat{w}(k)\hat{c}(k)\rho\hat{h}(k), \tag{2}$$

where h is the total correlation function, c is the direct cor-

relation function, ρ is the number density of molecules in the system, and w reflects the structure of the molecules and is given by

$$\hat{w}_{\alpha\gamma}(k)=\frac{\sin(kl_{\alpha\gamma})}{kl_{\alpha\gamma}}, \tag{3}$$

where $l_{\alpha\gamma}$ is the distance between sites α and γ in a molecule.

The SSOZ equation provides a relation between two unknowns, the total correlation function, h, and the direct correlation function, c. Therefore, another relation is needed in order to solve for h and c. It is in this additional equation, known as the closure relation, that approximations enter into the theory.

One commonly utilized approximate closure, the Percus–Yevick (PY) closure, is given by[20]

$$1+h_{\alpha\gamma}(r)=[1+f_{\alpha\gamma}(r)][1+h_{\alpha\gamma}(r)-c_{\alpha\gamma}(r)]. \tag{4}$$

The function, f, in Eq. (4) is known as the Mayer f function, and is given by $f_{\alpha\gamma}(r)=\exp[-\beta u_{\alpha\gamma}(r)]-1$, where $u_{\alpha\gamma}(r)$ is the interaction potential between a site of type α and a site of type γ, $\beta=1/k_BT$, where k_B is the Boltzmann constant, and T is the absolute temperature.

Another approximate closure, the hypernetted-chain (HNC) closure, is given by[20]

$$1+h_{\alpha\gamma}(r)=[1+f_{\alpha\gamma}(r)]\exp[h_{\alpha\gamma}(r)-c_{\alpha\gamma}(r)]. \tag{5}$$

The SSOZ equation, combined with either the PY or HNC closures, has been found[20] to work well for a variety of molecular systems. In general, the HNC closure is found to work well for systems characterized by long-range interactions, whereas the PY closure is found to work well for systems characterized by only short-range interactions.[1] When the SSOZ equation fails to yield reasonable predictions, there is no straightforward, systematic manner to improve its predictive accuracy. This shortcoming led to the development of the Chandler–Silbey–Ladanyi (CSL) equations, which are described in the next section.

B. The Chandler–Silbey–Ladanyi equations

For a detailed description of the CSL equations, the reader is referred to Ref. 7. In matrix form and in momentum (k) space, the CSL equations can be expressed as follows:[7]

$$\hat{h}^o(k)=\hat{c}^o(k)+\hat{c}^o(k)\rho\hat{h}^o(k)+\hat{c}^o(k)\rho\hat{h}^l(k)+\hat{c}^r(k)\rho\hat{h}^o(k), \tag{6}$$

$$\hat{h}^l(k)=\hat{c}^l(k)+\hat{s}(k)\hat{h}^o(k)+\hat{c}^b(k)\rho\hat{h}^o(k)+\hat{c}^l(k)\rho\hat{h}^o(k)+\hat{c}^l(k)\rho\hat{h}^l(k), \tag{7}$$

$$\hat{h}^r(k)=\hat{c}^r(k)+\hat{c}^o(k)\hat{s}(k)+\hat{c}^o(k)\rho\hat{h}^b(k)+\hat{c}^o(k)\rho\hat{h}^r(k)+\hat{c}^r(k)\rho\hat{h}^r(k), \tag{8}$$

$$\hat{h}^b(k)=\hat{c}^b(k)+\hat{c}^l(k)\hat{s}(k)+\hat{s}(k)\hat{h}^r(k)+\hat{c}^l(k)\rho\hat{h}^r(k)+\hat{c}^b(k)\rho\hat{h}^r(k)+\hat{c}^l(k)\rho\hat{h}^b(k), \tag{9}$$

where $h^i_{\alpha\gamma}(r)$ $[c^i_{\alpha\gamma}(r)]$ ($i=o$, l, r, or b) is the contribution to the site–site total [direct] correlation function associated with the ith group of diagrams. A caret (^) denotes the Fourier transform of a function. Each of the functions appearing in Eqs. (6)–(9) is a $n\times n$ matrix, where n is the number of interaction sites on the molecule. The matrix, ρ, is diagonal, and its elements are equal to the number densities of each of the sites in the system. The matrix, s, describes the geometrical arrangement of the interaction sites of the molecules comprising the system, and is given by

$$\hat{s}_{\alpha\gamma}(k)=(1-\delta_{\alpha\gamma})\,\frac{\sin(kl_{\alpha\gamma})}{kl_{\alpha\gamma}}, \tag{10}$$

where $l_{\alpha\gamma}$ is the distance between sites α and γ in a given molecule, and $\delta_{\alpha\gamma}$ is the Kronecker delta function.

As with the SSOZ equation, the CSL equations are not complete by themselves, and require additional closure relations. The corresponding closure relations are given by[10]

$$1+h^o_{\alpha\gamma}(r)=[1+f_{\alpha\gamma}(r)]e^{w^o_{\alpha\gamma}(r)}, \tag{11}$$

$$h^l_{\alpha\gamma}(r)=[1+f_{\alpha\gamma}(r)]e^{w^o_{\alpha\gamma}(r)}w^l_{\alpha\gamma}(r), \tag{12}$$

$$h^r_{\alpha\gamma}(r)=[1+f_{\alpha\gamma}(r)]e^{w^o_{\alpha\gamma}(r)}w^r_{\alpha\gamma}(r), \tag{13}$$

$$h^b_{\alpha\gamma}(r)=[1+f_{\alpha\gamma}(r)]e^{w^o_{\alpha\gamma}(r)}[w^l_{\alpha\gamma}(r)w^r_{\alpha\gamma}(r)+w^b_{\alpha\gamma}(r)], \tag{14}$$

where the site–site thermal correlation functions, $w^i_{\alpha\gamma}(r)$ ($i=o$, l, r, or b), are given by

$$w^o_{\alpha\gamma}(r)=t^o_{\alpha\gamma}(r)+b^o_{\alpha\gamma}(r), \tag{15}$$

$$w^l_{\alpha\gamma}(r)=t^l_{\alpha\gamma}(r)+b^l_{\alpha\gamma}(r), \tag{16}$$

$$w^r_{\alpha\gamma}(r)=t^r_{\alpha\gamma}(r)+b^r_{\alpha\gamma}(r), \tag{17}$$

$$w^b_{\alpha\gamma}(r)=t^b_{\alpha\gamma}(r)+b^b_{\alpha\gamma}(r), \tag{18}$$

where $t^i_{\alpha\gamma}(r)=h^i_{\alpha\gamma}(r)-c^i_{\alpha\gamma}(r)$ ($i=o$, l, r, or b) are the chain functions. The CSL equations, Eqs. (6)–(9), and their complementary closure relations, Eqs. (11)–(14), form a complete set of equations which can be solved to obtain the correlation functions of an interaction site fluid. The functions, $b^o_{\alpha\gamma}$, $b^l_{\alpha\gamma}$, $b^r_{\alpha\gamma}$, and $b^b_{\alpha\gamma}$, are the bridge functions, which are complex functionals of the correlation functions. As in the case of the simple fluids, the precise dependence of the bridge functions on the Mayer f functions is formally known.[21,9] However, these functions are too complex to be evaluated exactly, and therefore, approximations must be made to actually compute the site–site total correlation functions. One such approximation, which will be described in Sec. III, is the hypernetted-chain (HNC) approximation, in which the bridge functions are set equal to zero. In the next section, we discuss in detail several aspects of the bridge functions.

III. APPROXIMATION OF THE BRIDGE FUNCTIONS

The bridge functions are complicated functionals of the Mayer f functions. The precise dependence of the bridge functions on the Mayer f functions and the density is formally known[10] in diagrammatic terms. Specifically,

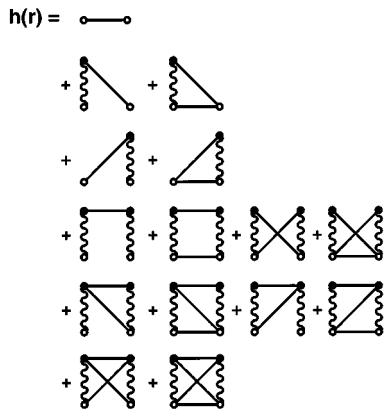

FIG. 1. The interaction site diagrams contributing to h at zeroth order in the density for a diatomic fluid. The straight lines represent Mayer f bonds, and the wavy lines represent s bonds. The white circles represent root sites, and the black circles represent field sites. The diagram on the first line contributes to h^o. The two diagrams on the second line contribute to h^l, the two diagrams on the third line contribute to h^r, and the remaining ten diagrams contribute to h^b.

$b^i(r)$ = subset of all diagrams in $h^i(r)$ which contain no f bonds between root circles, no articulation root pairs, and no nodal circles,

where $h^i(r)$ and $b^i(r)$ ($i=o$, l, r, or b) are the total correlation functions and the bridge functions, respectively. An articulation root pair is a pair of root circles that, when removed from a diagram, breaks the diagram into, at least, two disconnected parts where, at least, one of them does not contain a root circle.[9] For example, the pair of root (white) circles in the third diagram on the fourth row of Fig. 1 is an articulation root pair. A nodal circle is a circle through which all paths between a pair of root circles pass. For example, the black circle in the first diagram on the second row of Fig. 1 is a nodal circle. For a detailed explanation of the application of graph theory to both simple fluids and interaction site fluids, see Refs. 21 and 22, respectively.

In principle, the integrals corresponding to each of the diagrams contributing to $b^i(r)$ can be evaluated and summed up in order to obtain the bridge functions. In practice, however, two main problems prevent the actual implementation of this procedure. The first problem involves the enumeration of the diagrams which contribute to b^i, since the number of diagrams is, in fact, infinite. In addition, the number of diagrams present at each order of the density increases rapidly as the order of the density increases. The second problem involves the actual computation of the various integrals corresponding to each of the diagrams. Indeed, as the order of the diagrams increases, the dimension of the corresponding integrals increases by at least three (or even by more for multisite molecules) for each order of the density. For these reasons, the bridge functions cannot be evaluated exactly, and approximations must be made.

One of the simplest approximations is to neglect the bridge functions altogether, which leads to the well-known HNC closure. This approximation is fairly successful in the case of simple fluids. On the other hand, the HNC approximation for interaction site fluids is not as good. This reflects the fact that while the OZ-HNC equation is exact to first order in the density, the CSL-HNC equations are not exact even at zero density because the bridge functions b^l, b^r, and b^b include diagrams which are zeroth order in the density and higher. Note that for molecules having less than three interaction sites, the bridge functions b^l and b^r do not contain any diagrams which are zeroth order in the density, while the function b^o contains diagrams which are first order and higher in the density. On the other hand, the bridge functions corresponding to simple fluids contain diagrams which are second order and higher in the density. Since an integral equation becomes more accurate at higher orders in the density, its predictive capabilities improve as higher-order terms are included. This is similar to what happens in the case of the virial expansion for the equation of state, which becomes more accurate as higher-order virial coefficients are included. For this reason, the predictions of the CSL-HNC equations for interaction site fluids are not expected to be as accurate as those of the OZ-HNC equation for simple fluids.

The diagrams contributing to the bridge functions can be expressed as a power series in the density. Therefore, the next level of approximation to the CSL-HNC equations is to expand the bridge functions in powers of the density and compute the low-order terms. Mathematically, this involves writing the bridge functions as follows:

$$b^o_{\alpha\gamma}(r)=b^{o,(0)}_{\alpha\gamma}(r)+\rho b^{o,(1)}_{\alpha\gamma}(r)+\cdots , \tag{19}$$

$$b^l_{\alpha\gamma}(r)=b^{l,(0)}_{\alpha\gamma}(r)+\rho b^{l,(1)}_{\alpha\gamma}(r)+\cdots , \tag{20}$$

$$b^b_{\alpha\gamma}(r)=b^{b,(0)}_{\alpha\gamma}(r)+\rho b^{b,(1)}_{\alpha\gamma}(r)+\cdots , \tag{21}$$

and computing the functions $b^{i,(0)}_{\alpha\gamma}$, $b^{i,(1)}_{\alpha\gamma}$, etc., for $i=o$, l, r, or b. Note that the superscripts in parentheses denote the order of the density. *Note also that* $b^r_{\alpha\gamma}=b^l_{\gamma\alpha}$, *and, therefore, in the remainder of this paper, we will not present any equations referring to* b^r. To compute the bridge functions, the various bridge diagrams need to be enumerated. In the case of interaction site fluids, the number of bridge diagrams increases rapidly with the number of interaction sites present on the molecules. *When the CSL equations are combined with a closure which includes bridge diagrams of up to nth order in the density, we will refer to the resulting equations as the CSL-HNC+*$B^{(n)}$.

In order to calculate the low-order contributions to the bridge functions ($b^{i,(0)}_{\alpha\gamma}$, $b^{i,(1)}_{\alpha\gamma}$, etc.), we will develop a method to rewrite the diagrams in such a way that their number does not increase with the number of interaction sites, although the complexity (dimensionality) of each diagram may increase. This method is based on the observation that the interaction site diagrams arise[22] from molecular diagrams. *Note that interaction site diagrams deal explicitly with the actual sites that make up the molecules, and account*

for the individual interactions between sites on different molecules. On the other hand, molecular diagrams treat each molecule as a single entity and account for interactions between entire molecules.

We begin by writing the bridge functions in terms of the thermal, w^i, and chain, t^i, correlation functions as defined in Sec. II. At zeroth order in the density, the bridge functions are given by [see Eqs. (15)–(18)]

$$b_{\alpha\gamma}^{o,(0)}(r)=w_{\alpha\gamma}^{o,(0)}(r)-t_{\alpha\gamma}^{o,(0)}(r), \tag{22}$$

$$b_{\alpha\gamma}^{l,(0)}(r)=w_{\alpha\gamma}^{l,(0)}(r)-t_{\alpha\gamma}^{l,(0)}(r), \tag{23}$$

$$b_{\alpha\gamma}^{b,(0)}(r)=w_{\alpha\gamma}^{b,(0)}(r)-t_{\alpha\gamma}^{b,(0)}(r). \tag{24}$$

The first-order bridge functions are given by [see Eqs. (15)–(18)]

$$b_{\alpha\gamma}^{o,(1)}(r)=w_{\alpha\gamma}^{o,(1)}(r)-t_{\alpha\gamma}^{o,(1)}(r), \tag{25}$$

$$b_{\alpha\gamma}^{l,(1)}(r)=w_{\alpha\gamma}^{l,(1)}(r)-t_{\alpha\gamma}^{l,(1)}(r), \tag{26}$$

$$b_{\alpha\gamma}^{b,(1)}(r)=w_{\alpha\gamma}^{b,(1)}(r)-t_{\alpha\gamma}^{b,(1)}(r). \tag{27}$$

The indirect correlation functions can be written more compactly than the thermal correlation functions. Therefore, in order to simplify the computation of the thermal correlation functions, $w_{\alpha\gamma}^{i}(r)$ $(i=o,l,r,b)$, we rewrite these functions in terms of the indirect correlation functions, $y_{\alpha\gamma}^{i}(r)$ $(i=o,l,r,b)$, using the following definitions:

$$y_{\alpha\gamma}^{o}(r)=e^{w_{\alpha\gamma}^{o}(r)}, \tag{28}$$

$$y_{\alpha\gamma}^{o}(r)+y_{\alpha\gamma}^{l}(r)=e^{w_{\alpha\gamma}^{o}(r)}[1+w_{\alpha\gamma}^{l}(r)], \tag{29}$$

$$y_{\alpha\gamma}(r)=e^{w_{\alpha\gamma}^{o}(r)}\{[1+w_{\alpha\gamma}^{l}(r)][1+w_{\alpha\gamma}^{r}(r)]+w_{\alpha\gamma}^{b}(r)\}, \tag{30}$$

where $y_{\alpha\gamma}(r)=y_{\alpha\gamma}^{o}(r)+y_{\alpha\gamma}^{l}(r)+y_{\alpha\gamma}^{r}(r)+y_{\alpha\gamma}^{b}(r)$.

Expanding the indirect and thermal correlation functions in Eqs. (28)–(30) in powers of the density, and equating terms of the same order in the density, one finds that the zeroth-order thermal correlation functions are given by

$$w_{\alpha\gamma}^{o,(0)}(r)=0, \tag{31}$$

$$w_{\alpha\gamma}^{l,(0)}(r)=y_{\alpha\gamma}^{l,(0)}(r), \tag{32}$$

$$w_{\alpha\gamma}^{b,(0)}(r)=y_{\alpha\gamma}^{(0)}(r)-[1+y_{\alpha\gamma}^{l,(0)}(r)][1+y_{\alpha\gamma}^{r,(0)}(r)] \tag{33}$$

and that the first-order thermal correlation functions are given by

$$w_{\alpha\gamma}^{o,(1)}(r)=y_{\alpha\gamma}^{o,(1)}(r), \tag{34}$$

$$w_{\alpha\gamma}^{l,(1)}(r)=y_{\alpha\gamma}^{o,(1)}(r)+y_{\alpha\gamma}^{l,(1)}(r)-w_{\alpha\gamma}^{o,(1)}(r)[1+w_{\alpha\gamma}^{l,(0)}(r)], \tag{35}$$

$$w_{\alpha\gamma}^{b,(1)}(r)=y_{\alpha\gamma}^{(1)}(r)-w_{\alpha\gamma}^{l,(1)}(r)[1+w_{\alpha\gamma}^{r,(0)}(r)] -[1+w_{\alpha\gamma}^{l,(0)}(r)]w_{\alpha\gamma}^{r,(1)}(r). \tag{36}$$

The indirect correlation functions at each order in the density can be written as a sum of integrals, each of which can be represented by a diagram. To obtain these diagrams, we first examine those which contribute to the molecular total correlation function. These diagrams are typically written in terms of molecular f bonds, where $f_{\alpha\gamma}(r)=e_{\alpha\gamma}(r)-1$, and $e_{\alpha\gamma}$ is a site–site e bond, given by $e_{\alpha\gamma}(r)=\exp[-\beta u_{\alpha\gamma}(r)]$. However, it is more convenient in this case to use molecular e bonds. The molecular e bond, $e(R_1,R_2)=\exp[-\beta u(R_1,R_2)]$, can then be written as a product of site–site e bonds as follows

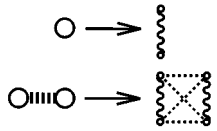

FIG. 2. The dependence of the molecular e bond on the site–site e bonds for a system of diatomic molecules. The thick dashed line represents the molecular e bond, the thin dashed lines represent the site–site e bonds, and the wavy lines represent s bonds [see Eq. (10)]. The large white circles represent molecular root sites, and the small white circles represent (interaction site) root sites.

$$e(R_1,R_2)=\prod_{\alpha\gamma} e_{\alpha\gamma}(r_1^{\alpha},r_2^{\gamma}), \tag{37}$$

where R_1 (R_2) denotes the position and orientation of molecule 1 (2), and r_1^{α} (r_2^{γ}) denotes the position of site α (γ) on molecule 1 (2). The molecular e bond is depicted diagrammatically in Fig. 2 for a system of diatomic molecules. Note that Eq. (37) is a direct manifestation of the fact that for an interaction site fluid, the interaction potential between two molecules, $u(R_1,R_2)$, can be written as

$$u(R_1,R_2)=\sum_{\alpha\gamma} u_{\alpha\gamma}(r_1^{\alpha},r_2^{\gamma}), \tag{38}$$

where $u_{\alpha\gamma}(r_1^{\alpha},r_2^{\gamma})$ is the interaction potential between site α in molecule 1 and site γ in molecule 2.

To obtain the interaction site diagram which contributes to the site–site correlation function from the corresponding molecular diagram, one just integrates over all sites which are not chosen to be root sites. Note that root sites are those sites between which one wants to know the correlations. An illustration of this procedure is presented in Fig. 3. Beginning with the molecular diagram on the left-hand side of the third row of Fig. 3, one expands the molecular circles to s-component bonds, and the molecular e bonds to site–site e

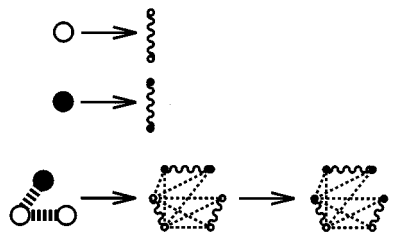

FIG. 3. Illustration of the procedure involved in obtaining an interaction site diagram from a molecular diagram. The notation is the same as that in Fig. 2.

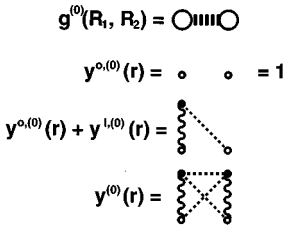

FIG. 4. Diagrams contributing to the zeroth-order molecular pair correlation function, $g^{(0)}(R_1,R_2)$, and the zeroth-order indirect correlation functions, $y^{o,(0)}$, $y^{o,(0)}+y^{l,(0)}$, and $y^{(0)}$. The thick dashed line represents a molecular e bond, the thin dashed lines represent site–site e bonds, and the wavy lines represent s bonds. The white circles represent root sites, and the black circles represent field sites.

bonds. In order to obtain the site–site correlation function between two sites, the bottom two white circles of the second diagram are chosen to be root circles, and the remaining white circles are darkened.

Using this procedure, one can obtain the diagrams which contribute to the site–site total correlation function from the diagrams which contribute to the molecular total correlation function. Finally, to obtain the diagrams which contribute to the site–site indirect correlation function, one rewrites Eqs. (28)–(30) as

$$y^i(r)=\delta_{i,o}+\text{subset of all diagrams in } h^i(r) \text{ which contain no } f \text{ bonds between root circles,}$$

where $i=o$, l, r, or b. The diagrams contributing to the zeroth-order indirect correlation functions are shown in Fig. 4, and those contributing to the first-order indirect correlation functions are shown in Fig. 5.

The chain functions can also be written as a sum of diagrams. To determine the relevant diagrams, we first rewrite the CSL equations [see Eqs. (6)–(9)] as

$$\hat{t}^o(k)=\hat{c}^o(k)\rho\hat{h}^o(k)+\hat{c}^o(k)\rho\hat{h}^l(k)+\hat{c}^r(k)\rho\hat{h}^o(k), \quad (39)$$

$$\hat{t}^l(k)=\hat{s}(k)\hat{h}^o(k)+\hat{c}^b(k)\rho\hat{h}^o(k)+\hat{c}^l(k)\rho\hat{h}^o(k)+\hat{c}^l(k)\rho\hat{h}^l(k), \quad (40)$$

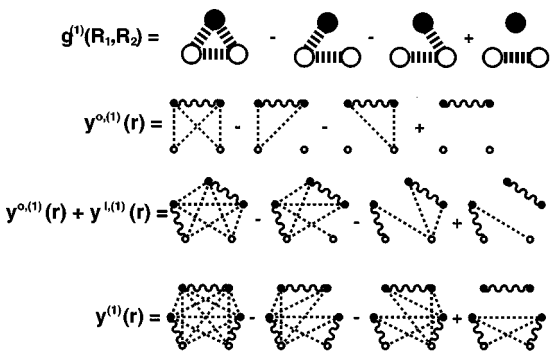

FIG. 5. Diagrams contributing to the first-order molecular pair correlation function, $g^{(1)}(R_1,R_2)$, and the first-order indirect correlation functions, $y^{o,(1)}$, $y^{o,(1)}+y^{l,(1)}$, and $y^{(1)}$. The notation is the same as that in Fig. 4.

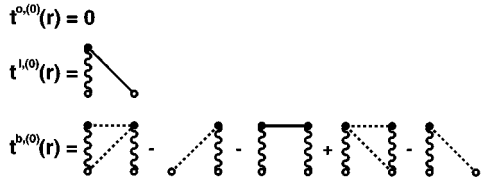

FIG. 6. Diagrams contributing to the zeroth-order chain functions for diatomic molecules. The solid lines represent Mayer f bonds, the dashed lines represent e bonds, and the wavy lines represent s bonds. The white circles represent root sites, and the black circles represent field sites.

$$\hat{t}^b(k)=\hat{c}^l(k)\hat{s}(k)+\hat{s}(k)\hat{h}^r(k)+\hat{c}^l(k)\rho\hat{h}^r(k)+\hat{c}^b(k)\rho\hat{h}^r(k)+\hat{c}^l(k)\rho\hat{h}^b(k). \quad (41)$$

Expanding Eqs. (39)–(41) in powers of the density, and collecting terms of zeroth order in the density yields

$$\hat{t}^{o,(0)}(k)=0, \quad (42)$$

$$\hat{t}^{l,(0)}(k)=\hat{s}(k)\hat{h}^{o,(0)}(k), \quad (43)$$

$$\hat{t}^{b,(0)}(k)=\hat{c}^{l,(0)}(k)\hat{s}(k)+\hat{s}(k)\hat{h}^{r,(0)}(k). \quad (44)$$

Similarly, collecting terms of first order in the density yields

$$\hat{t}^{o,(1)}(k)=\hat{c}^{o,(0)}(k)\hat{h}^{o,(0)}(k)+\hat{c}^{o,(0)}(k)\hat{h}^{l,(0)}(k)+\hat{c}^{r,(0)}(k)\hat{h}^{o,(0)}(k), \quad (45)$$

$$\hat{t}^{l,(1)}(k)=\hat{s}(k)\hat{h}^{o,(1)}(k)+\hat{c}^{b,(0)}(k)\hat{h}^{o,(0)}(k)+\hat{c}^{l,(0)}(k)\hat{h}^{o,(0)}\times(k)+\hat{c}^{l,(0)}(k)\hat{h}^{l,(0)}(k), \quad (46)$$

$$\hat{t}^{b,(1)}(k)=\hat{c}^{l,(1)}(k)\hat{s}(k)+\hat{s}(k)\hat{h}^{r,(1)}(k)+\hat{c}^{l,(0)}(k)\hat{h}^{r,(0)}(k)+\hat{c}^{b,(0)}(k)\hat{h}^{r,(0)}(k)+\hat{c}^{l,(0)}(k)\hat{h}^{b,(0)}(k). \quad (47)$$

Substituting the diagrammatic expansions for the site–site total correlation functions in Eqs. (42)–(47), one obtains the diagrams which contribute to the chain functions at zeroth and first order in the density. The resulting diagrams which contribute to the chain functions for diatomic molecules at zeroth order in the density are shown in Fig. 6, and those which contribute at first order in the density are shown in Fig. 7. For molecules having more than two interaction sites, the number of diagrams does not increase, although the complexity (dimensionality) of each diagram increases.

Finally, substituting the diagrams which contribute to the thermal correlation functions and the chain functions (see Figs. 6 and 7) into Eqs. (22)–(27) yields the diagrams which contribute to the zeroth order and first order bridge functions (not shown due to space limitations).

So far, we have discussed a procedure for specifying the diagrams which contribute to the zeroth order and first order bridge functions. Next, these diagrams must be converted into integrals having the proper symmetry number, namely, the proper numerical prefactor multiplying each diagram. For complete details on this procedure, the reader is referred to Ref. 22. The integrals which appear at zeroth order are at most three dimensional. At first order, the integrals are six

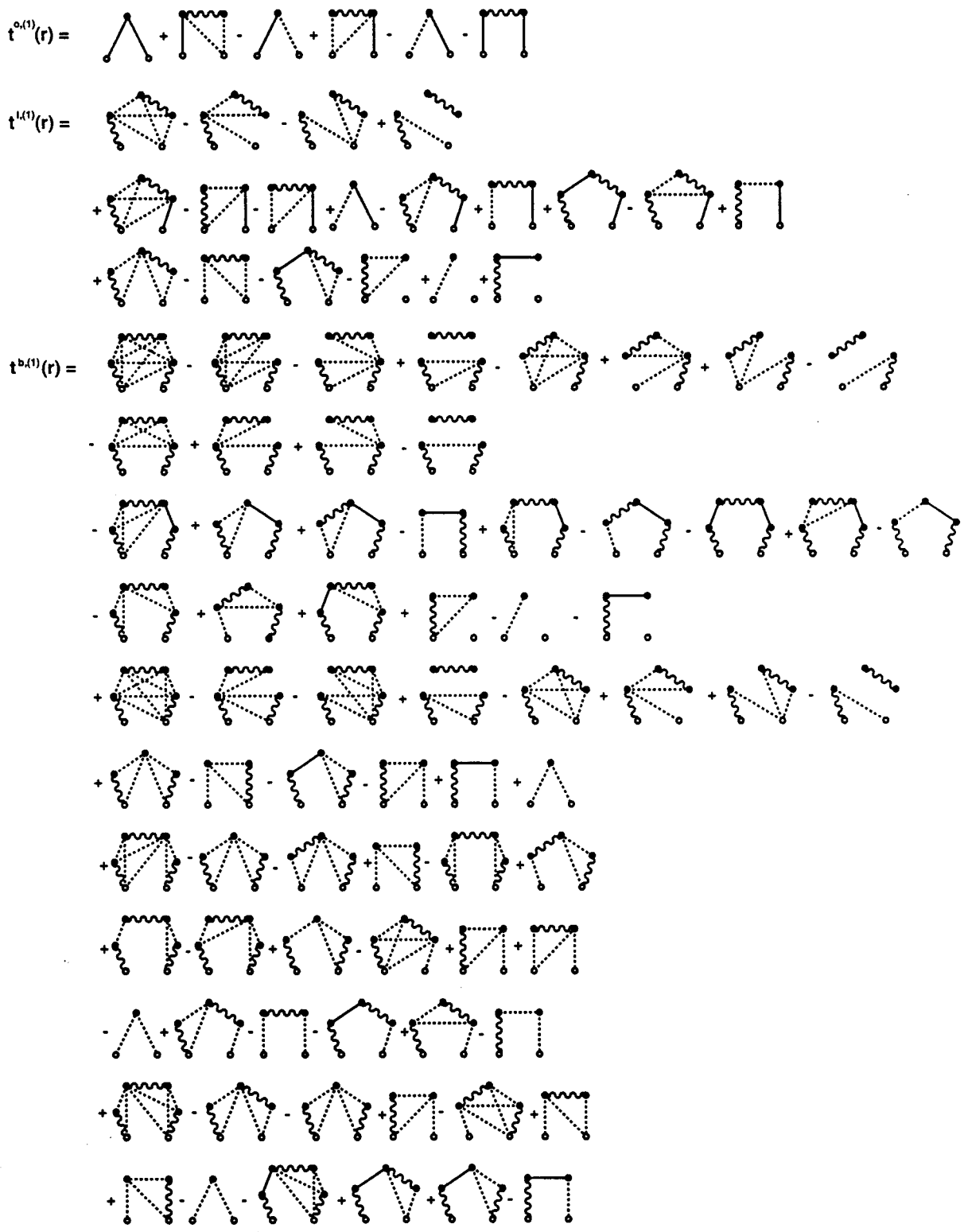

FIG. 7. Diagrams contributing to the first-order chain functions for diatomic molecules. The notation is the same as that in Fig. 6.

dimensional and lower. These integrals are performed using a Monte Carlo integration technique[23] for each value of r. In principle, the higher-order contributions to the bridge functions can also be computed using the method which we have outlined, but the calculations become extremely computationally expensive.

Next, we will apply the SSOZ-PY, CSL-HNC, CSL-HNC+$B^{(0)}$, and CSL-HNC+$B^{(1)}$ equations to three model systems: (i) homonuclear diatomic Lennard-Jones fluids (see Sec. IV A), (ii) nonpolar heteronuclear diatomic Lennard-Jones fluids (see Sec. IV B 1), and (iii) polar heteronuclear diatomic Lennard-Jones fluids (see Sec. IV B 2).

IV. RESULTS AND DISCUSSIONS

A. Homonuclear diatomic Lennard-Jones fluids

One of the simplest systems to model consists of diatomic fluids having two identical Lennard-Jones atoms rigidly connected to each other with their centers a distance, l, apart. The Lennard-Jones interaction potential, $u(r)$, is given by

$$u(r)=4\epsilon\left[\left(\frac{\sigma}{r}\right)^{12}-\left(\frac{\sigma}{r}\right)^{6}\right], \tag{48}$$

where ϵ characterizes the depth of the attractive interaction, and σ characterizes the width of the repulsive core. Three parameters are needed to uniquely specify the state of a system of homonuclear diatomic Lennard-Jones molecules: (i) the reduced temperature, $T^*=k_BT/\epsilon$, (ii) the reduced density, $\rho^*=\rho\sigma^3$, and (iii) the reduced bond length, $l^*=l/\sigma$. The structure and thermodynamics of these systems have been studied in the past using the SSOZ equation[24,25,5,26] as well as computer simulations.[27–30]

In the extended-atom (ea) limit, where the bond lengths become infinitely long, all the interaction sites are disconnected, and therefore, the interaction site fluid reduces to a simple fluid. In this limit, the CSL-HNC equations reduce to the Ornstein–Zernike equation with the HNC closure (OZ-HNC), and the SSOZ-PY equation reduces to the Ornstein–Zernike equation with the PY closure (OZ-PY). Note that both the OZ-HNC and OZ-PY equations work fairly well for simple fluids. On the other hand, in the united-atom (ua) limit, where all the bond lengths are equal to zero, and once again the system reduces to a simple fluid, neither of these integral equations reduces to a simple fluid equation. In view of these arguments, both the CSL and the SSOZ equations are expected to perform better for systems having longer bond lengths, that is, as the ea limit is approached.

We first solved the CSL-HNC equations and the SSOZ-PY equation at various values of T^*, ρ^*, and l^* to assess the range over which each of the integral equations yields accurate predictions of the fluid structure, as well as to identify which equation performs better. Both the CSL-HNC and the SSOZ-HNC equations were solved using an extension of the method developed by Labik *et al.*[31] The grid spacing was 0.025σ with 1024 grid points. The long-range interactions were handled using the method of Ng.[32]

To determine the accuracy of the predictions of the CSL-HNC and SSOZ-PY equations, we also performed computer simulations using the NVT Metropolis Monte Carlo method. The system consisted of 108 molecules with a potential cutoff of 3σ. Each simulation was started with an equilibration run of 1000 passes, and each pair correlation function was obtained using a run of 30 000 steps.

We first analyzed the influence of the fluid density on the accuracy of the predictions of the SSOZ and CSL equations. In Figs. 8 and 9, we show the predicted site–site pair correlation functions for homonuclear diatomic Lennard-Jones fluids having a bond length, $l^*=0.603$, for reduced densities of $\rho^*=0.1$ and $\rho^*=0.5$, at $T^*=3.0$. The solid lines are the predictions of the CSL-HNC equations, the dashed lines are the predictions of the SSOZ-PY equation, and the circles represent the results of our Monte Carlo simulations. At the higher densities (above the critical density, $\rho_c^*\approx 0.18$ for this particular system),[33] the SSOZ-PY predictions tend to be in better agreement with the simulation results than those of the CSL-HNC equations (see Fig. 9). However, as the density decreases, the SSOZ-PY equation tends to overpredict the pair correlation function, while the CSL-HNC equations tend to yield more accurate estimates (see Fig. 8). Examining reduced temperatures other than $T^*=3.0$ and bond lengths other than $l^*=0.603$ leads to a similar conclusion regarding the dependence on ρ^*. To summarize, for homonuclear diatomic fluids, the CSL-HNC equations will yield better predictions for the site–site pair correlation function than the SSOZ-PY equation when $\rho^*<\rho_c^*$, while the reverse holds when $\rho^*>\rho_c^*$.

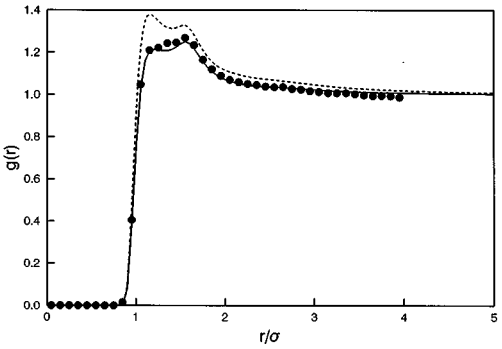

FIG. 8. Predicted site–site pair correlation function for homonuclear diatomic Lennard-Jones molecules at $T^*=3.0$, $\rho^*=0.1$, and $l^*=0.603$: (i) predicted using the CSL-HNC equations (solid line), (ii) predicted using the SSOZ-PY equation (dashed line), and (iii) predicted from our Monte Carlo simulations (circles).

Next, we examined the effect of bond length on the predictive capabilities of the CSL and SSOZ equations. In Figs. 9–11, we show the predicted site–site pair correlation functions of homonuclear diatomic Lennard-Jones molecules having bond lengths, $l^*=0.603$, 0.329, and 0.793, respectively. Note that varying l^* actually changes the phase behavior of the system, including its critical density and critical temperature. For each of the systems considered, ρ^* and T^* were chosen such that each system was in the liquid regime with a density well above the critical density. Accordingly,

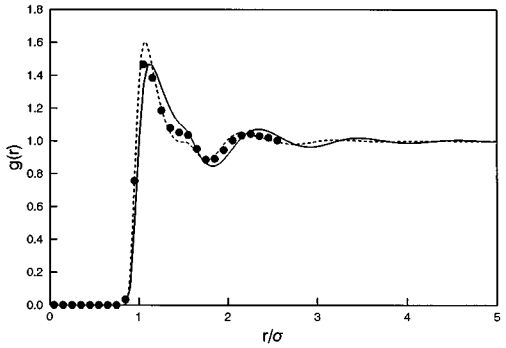

FIG. 9. Predicted site–site pair correlation function for homonuclear diatomic Lennard-Jones molecules at $T^*=3.0$, $\rho^*=0.5$, and $l^*=0.603$. The notation is the same as that in Fig. 8.

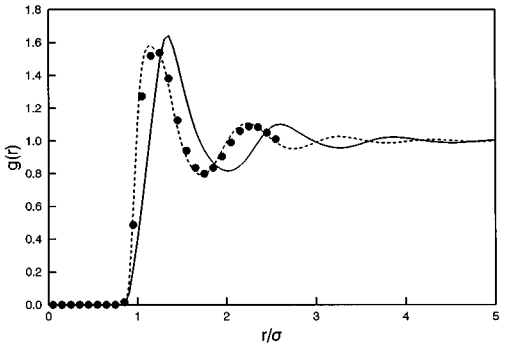

FIG. 10. Predicted site–site pair correlation function for homonuclear diatomic Lennard-Jones molecules at $T^*=3.0$, $\rho^*=0.55$, and $l^*=0.329$. The notation is the same as that in Fig. 8.

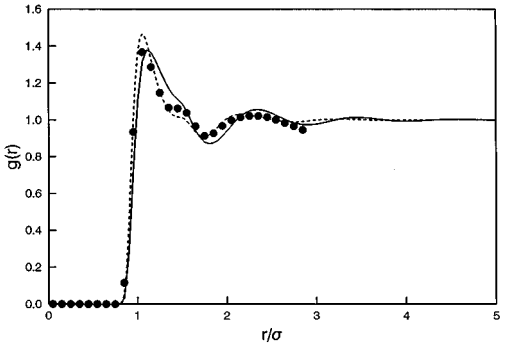

FIG. 12. Predicted site–site pair correlation function for homonuclear diatomic Lennard-Jones molecules at $T^*=5.0$, $\rho^*=0.5$, and $l^*=0.603$. The notation is the same as that in Fig. 8.

the SSOZ-PY equation is expected to perform better than the CSL-HNC equations, which is indeed the case. However, it is interesting to note that the predictions of the CSL-HNC equations improve significantly as l^* increases (see Fig. 11). On the other hand, the predictive capabilities of the SSOZ-PY equation seem to improve as l^* decreases (see Fig. 10). Once again, this trend for the dependence on l^* remains valid for other values of ρ^* and T^*.

Finally, we examined the effect of reduced temperature, T^*, on the predictions of the CSL-HNC and SSOZ-PY equations. Note that as the reduced temperature increases, the attractive interaction becomes less important, and the system behaves more like a fluid of symmetric hard dumbbells. In Figs. 9 and 12, we show the predicted site–site pair correlation functions for a homonuclear diatomic Lennard-Jones fluid with $\rho^*=0.5$ and $l^*=0.603$ for $T^*=3.0$ and 5.0, respectively. It is seen that temperature does not significantly influence the accuracy of the CSL-HNC equations. On the other hand, the predictions of the SSOZ-PY equation improve slightly with increasing temperature.

As mentioned in Sec. III, approximations enter the CSL-HNC equations through the neglect of the bridge functions. For simple fluids, the first bridge diagrams enter at second order in the density. However, for molecular fluids, the first bridge diagrams enter already at zeroth order in the density. Accordingly, the first correction to the CSL-HNC equations involves adding the zeroth-order bridge diagrams. The resulting integral equation for interaction site fluids is exact at zero density, which is not the case for either the CSL-HNC or SSOZ-PY equations. The predicted low-order density terms of the bridge functions for a homonuclear diatomic Lennard-Jones fluid at $T^*=3.0$, $\rho^*=0.5$, and $l^*=0.603$ are plotted in Fig. 13. The solid line is the function $b^{b,(0)}$, the dashed line is the function $\rho b^{o,(1)}$, the dotted line is the function $\rho b^{l,(1)}$, and the dashed–dotted line is the function $\rho b^{b,(1)}$. Note that $b^{o,(0)}$ [see Eqs. (22), (31), and (42)] and $b^{l,(0)}$ [see Eqs. (23), (32), and (43) and Fig. 6] are equal to zero for diatomic fluids, and therefore are not plotted. Note also that all the bridge functions are essentially zero for $r \geqslant 2\sigma$, which is consistent with the fact that they are short ranged.

In Fig. 14, we plot the predicted site–site pair correlation function for a system of homonuclear diatomic Lennard-Jones molecules at $T^*=3.0$, $\rho^*=0.5$, and $l^*=0.603$. The solid line is the prediction of the CSL-HNC equations, presented earlier in Fig. 9, the dashed line is the prediction of the CSL-HNC+$B^{(0)}$ equations, which includes the zeroth-order bridge diagrams, the dotted line is the prediction of the CSL-HNC+$B^{(1)}$ equations, which includes both the zeroth-order and the first-order bridge diagrams, the dashed–dotted line is the prediction of the SSOZ-PY equation, and the circles represent the results of our Monte Carlo simulations.

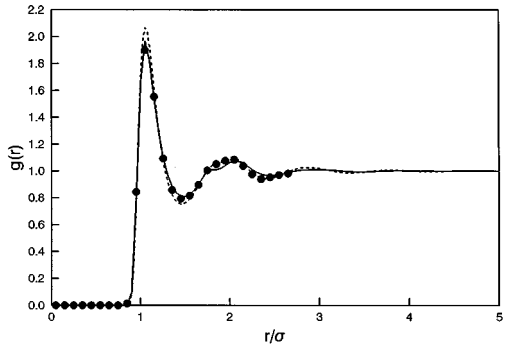

FIG. 11. Predicted site–site pair correlation function for homonuclear diatomic Lennard-Jones molecules at $T^*=2.0$, $\rho^*=0.5$, and $l^*=0.793$. The notation is the same as that in Fig. 8.

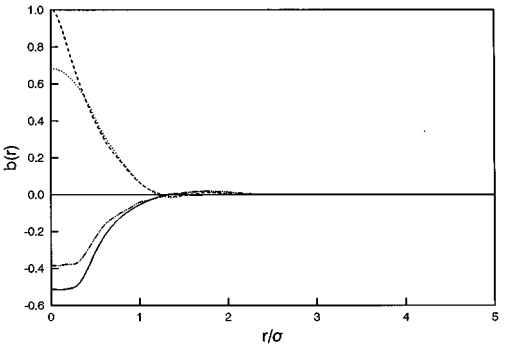

FIG. 13. Predicted bridge functions for homonuclear diatomic Lennard-Jones molecules at $T^*=3.0$, $\rho^*=0.5$, and $l^*=0.603$: (i) $b^{b,(0)}(r)$ (solid line), (ii) $\rho b^{o,(1)}(r)$ (dashed line), (iii) $\rho b^{l,(1)}(r)$ (dotted line), and $\rho b^{b,(1)}(r)$ (dashed–dotted line).

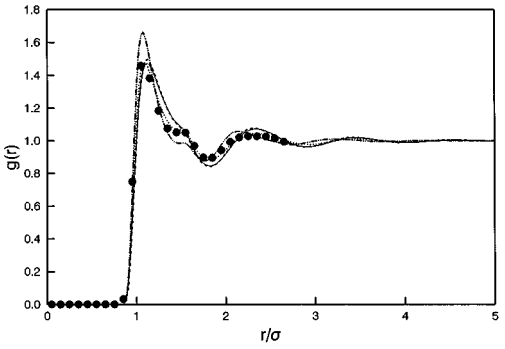

FIG. 14. Predicted site–site pair correlation function for homonuclear diatomic Lennard-Jones molecules at $T^*=3.0$, $\rho^*=0.5$, and $l^*=0.603$: (i) predicted using the CSL-HNC equations (solid line), (ii) predicted using the CSL-HNC+$B^{(0)}$ equations (dashed line), (iii) predicted using the CSL-HNC+$B^{(1)}$ equations (dotted line), (iv) predicted using the SSOZ-PY (dashed–dotted line) equations, and (v) predicted from our Monte Carlo simulations (circles). Note that the predictions of the CSL-HNC and CSL-HNC+$B^{(0)}$ equations are almost identical.

As can be seen, the addition of the zeroth-order bridge functions does not greatly alter the predictions of the CSL equations, and as a consequence, there is significant overlap between the solid and dashed lines. The addition of the first-order bridge diagrams, however, significantly improves the accuracy of the CSL equations. It is noteworthy, that the predictions of the CSL-HNC+$B^{(1)}$ equations are in better agreement with the simulation data than the predictions of the SSOZ-PY equation.

In Fig. 15, we plot the predicted site–site pair correlation function for a system of homonuclear diatomic Lennard-Jones molecules at $T^*=3.0$, $\rho^*=0.55$, and $l^*=0.329$. The predictions of the CSL-HNC (solid line) and CSL-HNC+$B^{(0)}$ (dashed line) equations are very similar. The predictions of the CSL-HNC+$B^{(1)}$ equations (dotted line) again represent an improvement over those of the CSL-HNC and CSL-HNC+$B^{(0)}$ equations. However, in the present case, they are inferior to those of the SSOZ-PY equation (dashed–dotted line), which is consistent with our earlier observation that the accuracy of the CSL equations worsens as l^* decreases. This, in turn, indicates that the higher-order bridge functions become more important for molecules having shorter bond lengths.

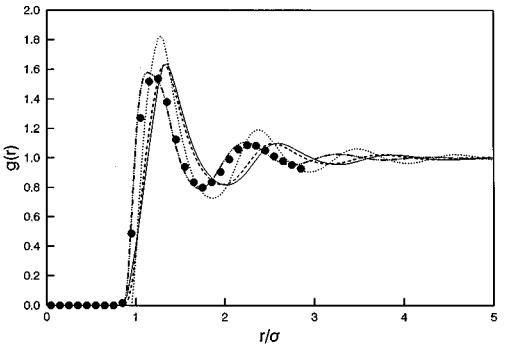

FIG. 15. Predicted site–site pair correlation function for homonuclear diatomic Lennard-Jones molecules at $T^*=3.0$, $\rho^*=0.55$, and $l^*=0.329$. The notation is the same as that in Fig. 14. Note that the predictions of the CSL-HNC and CSL-HNC+$B^{(0)}$ equations are almost identical.

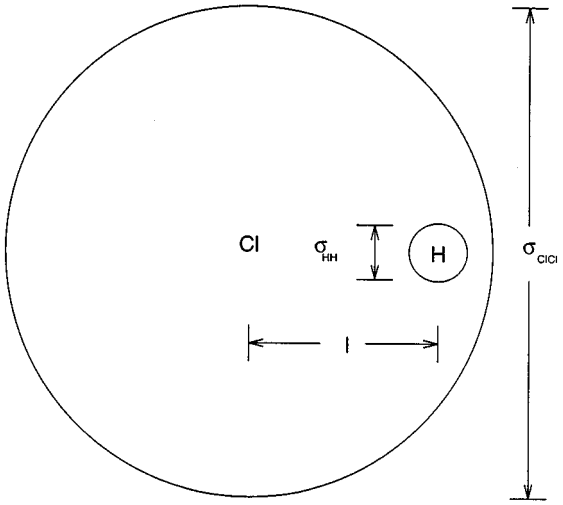

FIG. 16. Schematic drawing of the model HCl molecule.

In summary, the same trends which are observed for the CSL-HNC equations are also followed when the bridge functions are added. *Specifically, the predictions of the CSL equations become better for longer bond lengths and lower densities. In addition, the predictions of the CSL equations improve when higher-order bridge functions are included.*

B. Heteronuclear diatomic Lennard-Jones molecules

In this section, we evaluate the formalism presented in Sec. III in the case of heteronuclear diatomic Lennard-Jones molecules. Specifically, we consider a model for hydrogen chloride (HCl) which consists of two Lennard-Jones atoms having different sizes, which are rigidly connected to each other.[24] The interaction potential between sites α and γ, $u_{\alpha\gamma}(r)$, is given by[24]

$$u_{\alpha\gamma}(r)=4\epsilon_{\alpha\gamma}\left[\left(\frac{\sigma_{\alpha\gamma}}{r}\right)^{12}-\left(\frac{\sigma_{\alpha\gamma}}{r}\right)^{6}\right]+\frac{q_\alpha q_\gamma}{r}. \tag{49}$$

The parameters which describe this potential model are:[24] $\sigma_{HH}=0.4$ Å, $\epsilon_{HH}/k_B=20$ K, $q_H=0.2e$, $\sigma_{Cl}=3.353$ Å, $\epsilon_{Cl}/k_B=259$ K, $q=-0.2e$, and $l=1.3$ Å, where e is the elementary charge, and l is the distance between the two interactions sites. The cross-interaction terms are given by[24]

$$\sigma_{\alpha\gamma}=\tfrac{1}{2}(\sigma_{\alpha\alpha}+\sigma_{\gamma\gamma}), \tag{50}$$

$$\epsilon_{\alpha\gamma}=\sqrt{\epsilon_{\alpha\alpha}\epsilon_{\gamma\gamma}}. \tag{51}$$

An interesting feature of this molecule is that the smaller interaction site (H) is fully enclosed by the larger interaction site (Cl). A schematic drawing of this molecule is shown in Fig. 16.

1. Nonpolar molecules

Initially, we examined this model without the charges, namely, we set $q_H=q_{Cl}=0$ in Eq. (49). The CSL equations with the HNC, HNC+$B^{(0)}$, and HNC+$B^{(1)}$ closures, and the

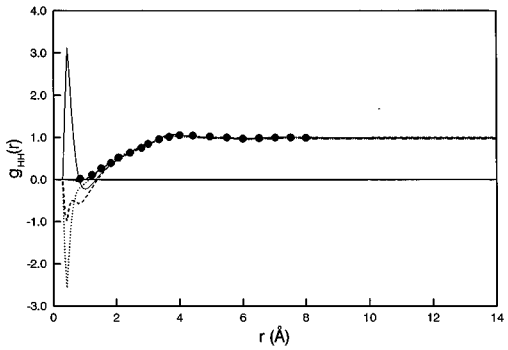

FIG. 17. Predicted hydrogen–hydrogen pair correlation function for uncharged HCl at $T=210$ K and $\rho=0.018$ Å^{-3}: (i) predicted using the CSL-HNC equations (solid line), (ii) predicted using the CSL-HNC+B$^{(0)}$ equations (dashed line), (iii) predicted using the CSL-HNC+B$^{(1)}$ equations (dotted line), (iv) predicted using the SSOZ-PY equation (dashed–dotted line), and (v) predicted from molecular dynamics simulations of Hirata *et al.* (Ref. 24) (circles). Note that the predictions of the CSL-HNC and CSL-HNC+B$^{(0)}$ equations are almost identical.

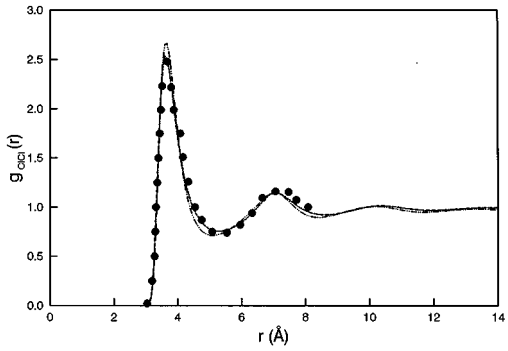

FIG. 19. Predicted chlorine–chlorine pair correlation function for uncharged HCl at $T=210$ K and $\rho=0.018$ Å^{-3}. The notation is the same as that in Fig. 17. Note that the predictions of the CSL-HNC and CSL-HNC+B$^{(0)}$ equations are almost identical.

SSOZ equation with the HNC closure were solved using an extension of the method of Labik.[31] This time, however, the grid consisted of 2048 points with $\Delta r=0.036$ Å. The predicted site–site pair correlation functions of this system, g_{HH}, g_{HCl}, and g_{ClCl}, at $T=210$ K and $\rho=0.018$ Å^{-3} (the same conditions used in the computer simulations of Hirata *et al.*)[24] are plotted in Figs. 17–19, respectively. The solid lines are the predictions of the CSL-HNC equations, the dashed lines are the predictions of the CSL-HNC+B$^{(0)}$ equations, the dotted lines are the predictions of the CSL-HNC+B$^{(1)}$ equations, the dashed–dotted lines are the predictions of the SSOZ-PY equation, and the circles represent the simulation data of Hirara *et al.*[24] As in the case of the homonuclear diatomic fluids, *the predictions of the CSL-HNC equations are very similar to those of the CSL-HNC+B$^{(0)}$ equations, and as a result, there is much overlap between the solid and dashed lines*.

The CSL-HNC equations are in closest agreement with the simulation data for the Cl–Cl pair correlation function (see Fig. 19), although the SSOZ-PY predictions are fairly similar. With the exception of the observed small negative region near $r=2$ Å, the predictions of the CSL-HNC equations and the SSOZ-PY equation are in close agreement with the computer simulation data for $g_{HCl}(r)$ (see Fig. 18). The negative region predicted by the SSOZ-PY equation is much less pronounced than that predicted by the CSL-HNC equations. Note also, that the addition of the bridge functions tends to decrease the magnitude of the negative region.

For $g_{HH}(r)$ (see Fig. 17), the predictions of the four integral equations are all in close agreement with the computer simulation results for $r\geqslant 2$ Å. However, for both $g_{HH}(r)$ and $g_{HCl}(r)$ (see Figs. 17 and 18, respectively) there are a few unphysical features predicted by the CSL-HNC equations. First, there is a negative region present in the H–H and H–Cl pair correlation functions. This feature is also predicted by the SSOZ-PY equation. Another unphysical prediction of the CSL-HNC equations is the presence of a sharp peak at about 0.4 Å in the H–H pair correlation function.

It is interesting to discuss possible sources of these unphysical predictions. To gain a better understanding of this problem, let us examine the predictions of the CSL-HNC equations for the individual h-component bonds (see Figs. 20–22). Note that the function $h^{l}_{\alpha\gamma}$ is associated with the correlations between a site α located within a molecule and a

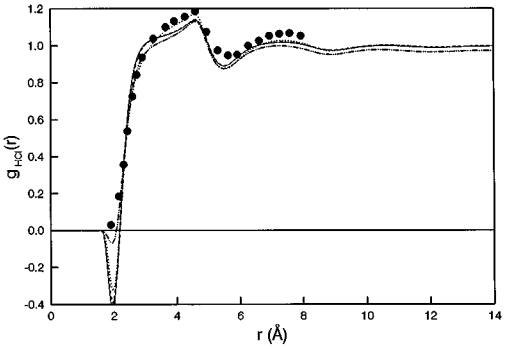

FIG. 18. Predicted hydrogen–chlorine pair correlation function for uncharged HCl at $T=210$ K and $\rho=0.018$ Å^{-3}. The notation is the same as that in Fig. 17. Note that the predictions of the CSL-HNC and CSL-HNC+B$^{(0)}$ equations are almost identical.

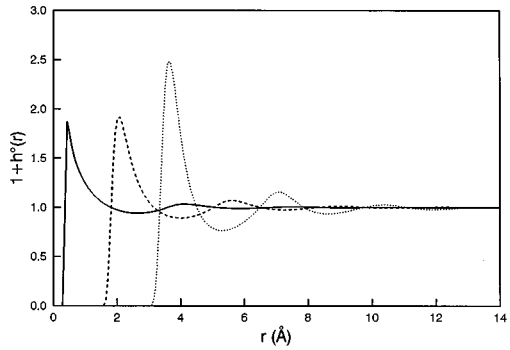

FIG. 20. Predicted behavior of h^{o} for uncharged HCl using the CSL-HNC equations: (i) $h^{o}_{HH}(r)$ (solid line), (ii) $h^{o}_{HCl}(r)$ (dashed line), and (iii) $h^{o}_{ClCl}(r)$ (dotted line).

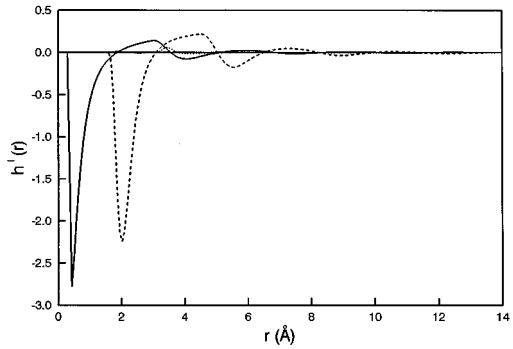

FIG. 21. Predicted behavior of h^l for uncharged HCl using the CSL-HNC equations: (i) $h^l_{\mathrm{HH}}(r)$ (solid line), (ii) $h^l_{\mathrm{HCl}}(r)$ (dashed line), (iii) $h^l_{\mathrm{ClCl}}(r)$ (dotted line), and (iv) $h^l_{\mathrm{ClH}}(r)$ (dashed–dotted line). Note that $h^l_{\mathrm{ClH}}(r)$ is nearly equal to zero.

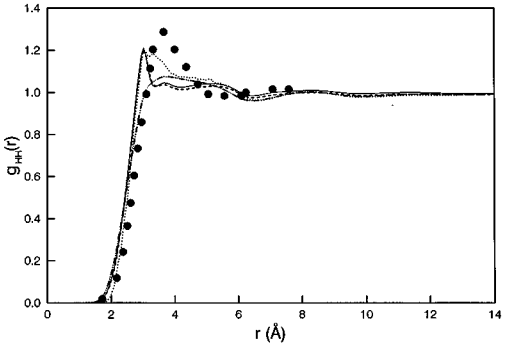

FIG. 23. Predicted hydrogen–hydrogen pair correlation function for charged HCl at $T=210$ K and $\rho=0.018$ Å^{-3}. The notation is the same as that in Fig. 17. Note that the predictions of the CSL-HNC and CSL-HNC+B$^{(0)}$ equations are almost identical.

disconnected site γ at infinite dilution in the bulk liquid. *Therefore, h^l is not a symmetric matrix, namely, $h^l_{\alpha\gamma}\neq h^l_{\gamma\alpha}$.* The same applies to c^l and b^l.

The first peak in the h^o_{HH} (see Fig. 20) and the h^b_{HH} (see Fig. 22) functions is located at the minimum of the H–H interaction potential. These peaks should be canceled out by the negative peaks in the h^l_{HH} and the h^r_{HH} ($=h^l_{\mathrm{HH}}$) functions (see Fig. 21). However, slight errors in the positions and heights of these peaks result in the creation of the anomalous peak and the negative region in the H–H pair correlation function. The addition of the low-order bridge functions overcompensates for the anomalous peak at 0.4 Å. The peak is eliminated, but it becomes a negative region. Higher-order bridge functions are needed to remove this negative region.

2. Polar molecules

Next, we examined the same system with the addition of charges, $+0.2e$ to H and $-0.2e$ to Cl. The predicted pair correlation functions of this system are shown in Figs. 23–25 where the solid lines are the predictions of the CSL-HNC equations, the dashed lines are the predictions of the CSL-HNC+B$^{(0)}$ equations, the dotted lines are the predictions of the CSL-HNC+B$^{(1)}$ equations, and the circles represent the simulation data of Hirata *et al.*[24] *Note that there is considerable overlap between the solid (CSL-HNC) and dashed lines (CSL-HNC+B$^{(0)}$).* For the H–H and Cl–Cl pair correlation functions, the SSOZ-HNC and the CSL-HNC equations are of comparable accuracy. The H–Cl potential no longer has an attractive region, and thus the peak in the corresponding correlation function disappears. However, for the H–Cl pair correlation function, the CSL-HNC equations seem to offer an improvement over the SSOZ-HNC equation. We see that both integral equations predict an anomalous peak at about 2 Å, which is much less prominent for the CSL-HNC equations.

To examine why this peak is predicted by the CSL-HNC equations, one must examine the h-component bonds, which are shown in Figs. 26–28. Recall that $h_{\alpha\gamma}(r)=h^o_{\alpha\gamma}(r)+h^l_{\alpha\gamma}(r)+h^r_{\alpha\gamma}(r)+h^b_{\alpha\gamma}(r)$. For this system, the H–Cl site–site interaction potential has a minimum located at about 2 Å, which is where the anomalous peak is also located. At this position, we see a large peak in h^o_{HCl} (see Fig. 26) which should be canceled out by the negative peaks in h^l_{HCl}, h^r_{HCl} ($=h^l_{\mathrm{ClH}}$) (see Fig. 27), and h^b_{HCl} (see Fig. 28). The small errors in each of these functions, due to the approximations involved in using the HNC closure, causes this cancellation to be incomplete and leads to the creation of the anomolous peak in the H–Cl pair correlation function.

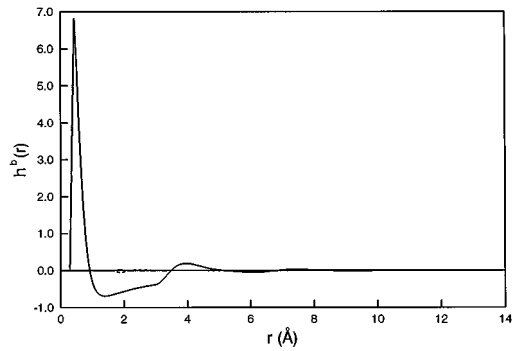

FIG. 22. Predicted behavior of h^b for uncharged HCl using the CSL-HNC equations: (i) $h^b_{\mathrm{HH}}(r)$ (solid line), (ii) $h^b_{\mathrm{HCl}}(r)$ (dashed line), and (iii) $h^b_{\mathrm{ClCl}}(r)$ (dotted line). Note that $h^b_{\mathrm{HCl}}(r)$ and $h^b_{\mathrm{ClCl}}(r)$ are essentially equal to zero.

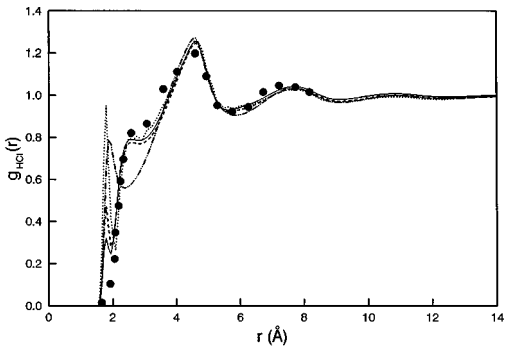

FIG. 24. Predicted hydrogen–chlorine pair correlation function for charged HCl at $T=210$ K and $\rho=0.018$ Å^{-3}. The notation is the same as that in Fig. 17. Note that the predictions of the CSL-HNC and CSL-HNC+B$^{(0)}$ equations are almost identical.

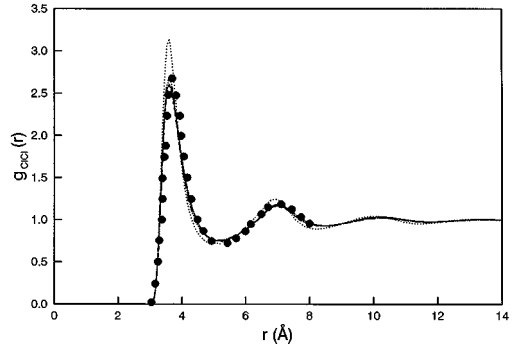

FIG. 25. Predicted chlorine–chlorine pair correlation function for charged HCl at $T=210$ K and $\rho=0.018$ Å^{-3}; the notation is the same as that in Fig. 17. Note that the predictions of the CSL-HNC and CSL-HNC+B$^{(0)}$ equations are almost identical.

The addition of the zeroth-order bridge functions (dashed lines) to the CSL-HNC equations does not significantly alter the predictions of the pair correlation functions. Adding the first-order bridge functions (see dotted lines) causes the height of the anomalous peak in g_{HCl} to increase, although, in general, it improves the agreement with the simulation data for all the pair correlation functions (see Figs. 23–25).

In general, the CSL equations tend to yield more accurate predictions for correlations between the larger interaction sites. This can be understood from the fact that the predictions of the CSL equations are independent of the presence of auxiliary sites, that is, sites which do not interact with other sites in the system, but only label positions within a molecule.[34] If the interactions between two molecules are governed primarily by one large interaction site, then the system can be approximated as a simple fluid. The correlations between these sites can be described quite accurately by the OZ equation, which is the limit approached by the CSL equations in this case. The other interaction sites, which are much smaller in comparison, can be viewed as being auxiliary sites. The correlations involving these interaction sites are also accounted for by the CSL equations, although not as accurately.

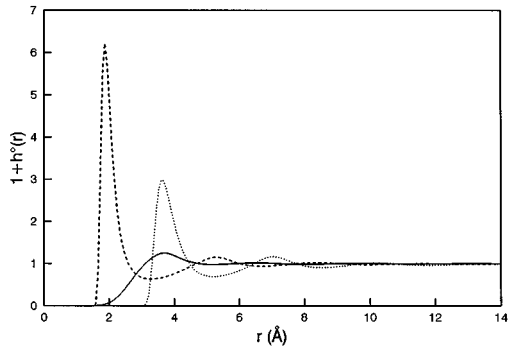

FIG. 26. Predicted behavior of h^o for charged HCl using the CSL-HNC equations: (i) $h^o_{\mathrm{HH}}(r)$ (solid line), (ii) $h^o_{\mathrm{HCl}}(r)$ (dashed line), and (iii) $h^o_{\mathrm{ClCl}}(r)$ (dotted line).

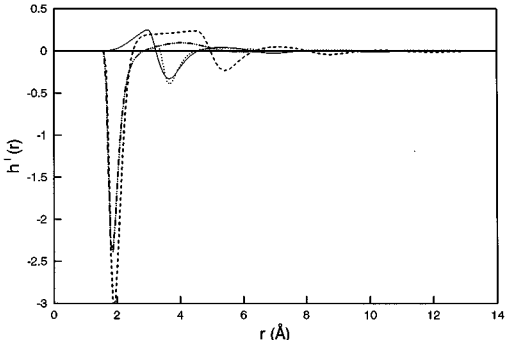

FIG. 27. Predicted behavior of h^l for charged HCl using the CSL-HNC equations: (i) $h^l_{\mathrm{HH}}(r)$ (solid line), (ii) $h^l_{\mathrm{HCl}}(r)$ (dashed line), (iii) $h^l_{\mathrm{ClCl}}(r)$ (dotted line), and (iv) $h^l_{\mathrm{ClH}}(r)$ (dashed–dotted line).

V. CONCLUSIONS

In this paper, we have compared the capabilities of the CSL-HNC and SSOZ-PY equations to predict pair correlation functions of homonuclear diatomic Lennard-Jones fluids at various temperatures, densities, and bond lengths. In general, the predictions of the CSL-HNC equations are in better agreement with the computer simulation results when the bond length increases or when the density decreases. Temperature does not have a significant effect on the structural predictive capabilities of these equations.

We have also presented a general method for computing the low-order density bridge functions. For the homonuclear Lennard-Jones molecules, the zeroth-order bridge functions were found to have little effect on the predictions of the CSL equations. However, the addition of the first-order bridge functions resulted in a significant improvement in the predictive capabilities of the CSL equations. The accuracy of these equations was found to increase with decreasing density and increasing bond length, similar to the situation encountered in the case of CSL-HNC equations.

We have also investigated the capabilities of the CSL-HNC and SSOZ-PY equations to predict the site–site pair correlation functions for heteronuclear diatomic Lennard-Jones fluids. For nonpolar molecules, the CSL-HNC equa-

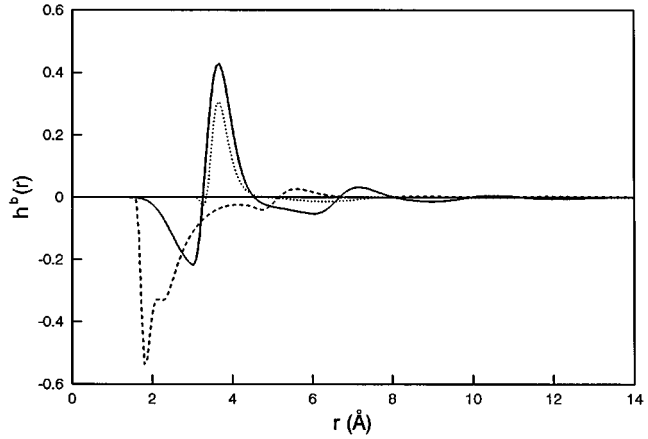

FIG. 28. Predicted behavior of h^b for charged HCl using the CSL-HNC equations: (i) $h^b_{\mathrm{HH}}(r)$ (solid line), (ii) $h^b_{\mathrm{HCl}}(b)$ (dashed line), and (iii) $h^b_{\mathrm{ClCl}}(r)$ (dotted line).

tions perform very well in predicting the correlation functions between the larger interaction sites. For the other correlation functions, the predictions of the CSL-HNC equations were found to be good for medium to large values of r. For separations around the atomic diameter, the CSL-HNC equations displayed anomalous behavior, including a negative region in $g(r)$. This is a consequence of the delicate nature of the cancellations which must occur between the h-component bonds. For polar diatomic molecules, the CSL-HNC equations seem to offer an improvement over the SSOZ-HNC equations. The CSL equations provide better predictions for correlation functions between the larger interaction sites.

We hope that the results presented in this paper will stimulate further application of the CSL equations in more complex cases. In fact, as shown, there are systems for which the CSL equations offer an improvement over the SSOZ equation. In particular, the success of the CSL-HNC equations in the case of charged diatomic molecules suggests that these equations may also work well for more complicated systems, such as water. Encouraged by these findings, we have recently applied[35] the CSL equations to various potential models of water to predict the structure, thermodynamics, and phase behavior of this complex fluid.

ACKNOWLEDGMENTS

This research was supported in part by the National Science Foundation (NSF) Presidential Young Investigator (PYI) Award to D.B., and a NSF Grant (No. DMR-84-18718) administered by the Center for Materials Science and Engineering at MIT. D.B. is grateful to BASF, Kodak, and Unilever for providing PYI matching funds. L.L. is grateful for the award of a NSF Graduate Fellowship.

[1] L. L. Lee, *Molecular Thermodynamics of Nonideal Fluids* (Butterworths, Boston, 1988).
[2] M. P. Allen and D. J. Tildesley, *Computer Simulation of Liquids* (Claredon, Oxford, 1987).
[3] D. E. Sullivan and C. G. Gray, Mol. Phys. **42**, 443 (1981).
[4] D. Chandler, C. G. Joslin, and J. M. Deutch, Mol. Phys. **47**, 871 (1982).
[5] C. S. Hsu, D. Chandler, and L. J. Lowden, Chem. Phys. **14**, 213 (1976).
[6] P. T. Cummings, C. G. Gray, and D. E. Sullivan, J. Phys. A **14**, 1483 (1981).
[7] D. Chandler, R. Silbey, and B. M. Ladanyi, Mol. Phys. **46**, 1335 (1982).
[8] D. Chandler, Mol. Phys. **31**, 1213 (1976).
[9] J. P. Hansen and I. R. McDonald, *Theory of Simple Liquids* (Academic, London, 1986).
[10] P. J. Rossky and R. A. Chiles, Mol. Phys. **51**, 661 (1984).
[11] M. Lupkowski and P. A. Monson, J. Chem. Phys. **87**, 3618 (1987).
[12] D. B. McGuigan, M. Lupkowski, D. M. Paquet, and P. A. Monson, Mol. Phys. **67**, 33 (1989).
[13] M. Lupkowski and P. A. Monson, Mol. Phys. **63**, 875 (1988).
[14] M. Lupkowski and P. A. Monson, Mol. Phys. **67**, 53 (1989).
[15] G. Dubey, S. F. O'Shea, and P. A. Monson, Mol. Phys. **80**, 997 (1993).
[16] L. Lue and D. Blankschtein, J. Chem. Phys. **100**, 3002 (1994).
[17] A. Yethiraj, Mol. Phys. **80**, 695 (1993).
[18] A. Yethiraj, R. Dickman, G. Szamel, E. Kierlik, and M.-L. Rosinberg, Mol. Phys. (submitted).
[19] D. Chandler and H. C. Andersen, J. Chem. Phys. **57**, 1930 (1972).
[20] F. Hirata and P. J. Rossky, Chem. Phys. Lett. **83**, 329 (1981).
[21] G. Stell, in *The Equilibrium Theory of Classical Fluids* (Benjamin, New York, 1964), pp. II–171.
[22] B. M. Ladanyi and D. Chandler, J. Chem. Phys. **62**, 4308 (1975).
[23] W. H. Press, S. A. Teukolsky, W. T. Vetterling, and B. P. Flannery, *Numerical Recipes in FORTRAN: The Art of Scientific Computing* (Cambridge University Press, Cambridge, 1992).
[24] F. Hirata, B. Montgomery Pettitt, and P. J. Rossky, J. Chem. Phys. **77**, 509 (1982).
[25] A. H. Narten, E. Johnson, and A. Habenschuss, J. Chem. Phys. **73**, 1248 (1980).
[26] P. A. Monson, Mol. Phys. **47**, 435 (1982).
[27] J. Barojas and D. Levesque, Phys. Rev. A **7**, 1092 (1973).
[28] P. S. Y. Cheung and J. G. Powles, Mol. Phys. **30**, 921 (1975).
[29] K. Singer, A. Taylor, and J. V. L. Singer, Mol. Phys. **33**, 1757 (1977).
[30] M. Wojcik, K. E. Gubbins, and J. G. Powles, Mol. Phys. **45**, 1209 (1982).
[31] S. Labik, A. Malijevsky, and P. Vonka, Mol. Phys. **56**, 709 (1985).
[32] K. Ng, J. Chem. Phys. **61**, 2680 (1974).
[33] G. M. Sowers and S. I. Sandler, Mol. Phys. **77**, 351 (1992).
[34] L. Lue and D. Blankschtein, J. Chem. Phys. (in press).
[35] L. Lue and D. Blankschtein, J. Chem. Phys. (in press).